Desalination and Water Treatment
www.deswater.com

doi: 10.1080/19443994.2016.1204365

57 (2016) 29509–29516
December

Taylor & Francis
Taylor & Francis Group

Photocatalytic degradation of bisphenol A by HMS/g-C_3N_4 composite

Lijun Luo[a,*], Wei Tang[a], Colin J. Barrow[c], Wenrong Yang[c], Hongbin Wang[a,*], Fengzhi Jiang[b]

[a] *Key Laboratory of Resource Clean Conversion in Ethnic Regions, Education Department of Yunnan, School of Chemistry and Environment, Yunnan MinZu University, Kunming 650500, China, Tel. +86 13629452541; Fax: +86 871 65910016; email: 10501931@qq.com (L. Luo), Tel. +86 18669010092; email: 317266182@qq.com (W. Tang), Tel. +86 13708440749; email: 595530820@qq.com (H. Wang)*

[b] *School of Chemical Science and Technology, Yunnan University, Kunming 650091, China, Tel. +86 13700661885; email: fengzhij@ynu.edu.cn*

[c] *Centre for Chemistry and Biotechnology, School of Life and Environmental Sciences, Deakin University, Waurn Ponds, Geelong, VIC 3216, Australia, Tel. +86 087165910017; email: colin.barrow@deakin.edu.au (C.J. Barrow), Tel. +61 3 5227 2932; email: wenrong.yang@deakin.edu.au (W. Yang)*

Received 8 December 2015; Accepted 14 June 2016

ABSTRACT

In this work, hexagonal mesoporous silica/g-C_3N_4 (HMS/C_3N_4) was synthesized by heating a mixture of self-prepared HMS and dicyandiamide. The as-prepared materials were characterized by transmission electron microscopy (TEM), X-ray diffractometer (XRD), Fourier transform infrared spectra (FT-IR) and Brunauer–Emmett–Teller analysis (BET). The prepared photocatalysts were applied to decompose bisphenol A (BPA) under UV light illumination. The mass ratios of HMS to melamine were optimized. The results showed that optimal mass ratios HMS to dicyandiamide was 1:1. Even though with the same catalyst dosage (1.0 g/L), the degradation kinetic rate constant of BPA over HMS/C_3N_4 ($0.00526\ \mathrm{min}^{-1}$) was 1.76 times and 1.4 times than those on P25 ($0.00298\ \mathrm{min}^{-1}$) and pure C_3N_4 ($0.00383\ \mathrm{min}^{-1}$), while the rate constant of photolysis was only $0.00021\ \mathrm{min}^{-1}$. The enhanced photocatalytic activity of the HMS/C_3N_4 composite was ascribed to higher specific surface area and less aggregation compared to the pure C_3N_4. It is feasible and efficient to degrade BPA by HMS/C_3N_4 composite, which is easier to be separated than pure C_3N_4 after the pollutant has been removed completely.

Keywords: Photocatalysis; g-C_3N_4; Mesoporous silica; Bisphenol A

1. Introduction

Semiconductor-based photocatalysis is considered to be an attractive way to challenge the worldwide energy shortage and environmental pollution issues. Polymeric graphitic carbon nitride (g-C_3N_4) is a novel emerging metal-free semiconductor with good physicochemical stability, non-toxicity and appropriate medium band gap (2.7 eV) [1–4]. In addition, g-C_3N_4 is

---

*Corresponding authors.

Presented at the 8th International Conference on Challenges in Environmental Science & Engineering (CESE-2015) 28 September–2 October 2015, Sydney, Australia

abundant and easily prepared via one-step polymerization from cheap chemicals like cyanamide [5], dicyandiamide [6], melamine [7], thiourea [8] and urea [9]. The C_3N_4 photocatalyst has extensively been studied in energy and environmental fields [10]. However, the prepared g-C_3N_4 usually has low specific surface area resulting in relative low photocatalytic activity. In order to solve this drawback, many researchers have prepared the porous C_3N_4 materials with a hard template method [11]. However, the method is complicated, requiring plenty of detrimental HF or NH_4HF to remove the hard template (SiO_2) [5,12]. There are also several works reporting that carbon nitrides with meso- or nano-porosity structure were synthesized by using a urea precursor [9,13]. But all in all, the pure g-C_3N_4 and porous C_3N_4 nanopowders are not easy to be separated and recycled after the photocatalytic experiment finishes. Mesoporous silicas have been commonly utilized as photocatalyst supporters to simplify the separation of the photocatalyst due to their high surface area and good sedimentation ability [14,15]. Moreover, it can enhance the photocatalytic activity of photocatalysts [16].

In this study, we propose a simple method to anchor g-C_3N_4 to self-made hexagonal mesoporous silica (HMS) to form hybrid material (denoted as HMS/C_3N_4) by heating a mixture of self-prepared HMS and dicyandiamide without eliminating the HMS with HF. The crystal phase structure, morphology, surface area and pore structure of the prepared HMS/g-C_3N_4 were studied in detail. The photocatalytic activity of HMS/g-C_3N_4 was evaluated by degrading the bisphenol A, which is a representative emerging endocrine disruptor chemical.

2. Experiments and methods

2.1. Materials

Tetraethoxysilance (TEOS, 99%) and dodecylamine (DDA) were purchased from Alfa Aesar Inc. Bisphenol A (BPA, purity 99%) was bought from Aldrich, Inc. HCl (35–37 wt%) was bought from Chengdu Kelong Chemical Reagent Factory, China. HPLC-grade acetonitrile was obtained from Merck Co., Ltd. All the reagents were analytical grade and were used as received. Ultrapure water (18.2 MΩ) used throughout the experiments was obtained from the laboratory purification system.

2.2. Synthesis of HMS/C_3N_4 composites

Hexagonal mesoporous silica (HMS) was prepared according to the method reported by Kuwahara et al. [17]. DDA (7.05 g) and 10% HCl solution (2.5 mL) were dissolved in deionized water (92 mL) under vigorous stirring for 1 h, and then the TEOS (29.3 g) dissolved in ethanol (53.7 mL) was slowly added to the mixture. The suspension was aged at room temperature for 24 h under stirring. The obtained precipitate was filtered, washed repeatedly with deionized water until neutral, and dried in air at 383 K overnight in vacuum. Then the as-synthesized sample was calcined at 823 K for 5 h to remove the DDA to form the hexagonal mesoporous silica (HMS). HMS/C_3N_4 composites were synthesized by simple mixing-calcination process of self-prepared HMS and dicyandiamide based on Hao Zhang's works with minor modification [14]. The heating rate was 2.3℃/min under 10 mL/min N_2 from room temperature to 550℃ and remained at 550℃ for 4 h. The HMS/C_3N_4 composites with different mass ratios of HMS to C_3N_4 were prepared by adjusting the mass ratio of HMS to dicyandiamide (5:7, 5:5, 5:4, 5:3, 5:2, and 5:1) and were denoted as HMS/7C_3N_4, HMS/5C_3N_4, HMS/4C_3N_4, HMS/3C_3N_4, HMS/2C_3N_4, and HMS/C_3N_4, respectively. Pure g-C_3N_4 powders were obtained by direct calcination of dicyandiamide at 550℃ for 4 h in muffle furnace.

2.3. Characterization of HMS/C_3N_4 composite

TEM samples were prepared by dispersing the powders in ethanol and depositing onto carbon-coated copper grids and morphology were observed on JEM-2100 transmission electron microscope (JEOL, Tokyo, Japan) with an acceleration voltage of 200 kV. X-ray diffraction patterns of HMS/C_3N_4 composites were obtained on a TTRIII X-ray diffractometer (Rigaku Corporation, Japan) with Cu Kα radiation in the 2θ range from 20° to 80° with scanning ratio of 10°/min and a step size of 0.02°/s, the accelerating voltage and the applied current were 40 kV and 250 mA, respectively. Fourier Transform Infrared spectra (FTIR) were conducted on a Nicolet iS10 FT-IR Spectrometer (Thermo Scientific, Germany) using KBr pellet technique over the wave number range of 4,000–400 cm^{-1} with a resolution of 2 cm^{-1}. Nitrogen (N_2) adsorption–desorption measurement at 77 K was conducted using TriStar II 3020 (Micromeritics Inc., USA). The surface area of samples was obtained using the Brunauer–Emmett–Teller (BET) plot of N_2 adsorption isotherm. The average pore volumes were calculated by using Barrett–Joyner–Halenda (BJH) method with the adsorption branch of the N_2 isotherm.

2.4. Photocatalytic degradation experiments

Batch experiments were carried out in XPA-7 photochemical Reactor (Xujiang electro-mechanical plant, Nangjing, China) to investigate photocatalytic performance for BPA. The ultraviolent light was provided by a 20 W UV lamp (λ = 254 nm). The reaction system was cooled by circulating water and maintained at room temperature. Typically, 0.0500 g of the prepared HMS/C_3N_4 was added into 50.00 mL of BPA aqueous solution (5 mg/L). Before illumination, the suspensions were stirred in dark for 30 min to reach the adsorption/desorption equilibrium on the photocatalyst surface, and the concentration of the BPA was detected as the initial concentration C_0. Then light illumination started and quartz tube containing 50.00 mL of BPA was taken out at scheduled time intervals and its concentration was determined as C_t. The suspension was immediately filtered through a 0.45 μm glass fiber filter to remove the catalyst particles and subjected to subsequent HPLC analysis. HPLC analysis conditions were selected according to our previous report [18].

In order to investigate the BPA degradation process over the prepared HMS/C_3N_4 hybrid materials, the experimental data were fitted by pseudo-first-order model. Its equation can be written in a linear form shown in Eq. (1):

$$\ln \frac{C_t}{C_0} = -\kappa t \qquad (1)$$

where C_0 is the initial concentration, C_t is the concentration of BPA after time (t), the slope of the fitted line of $\ln(C_t/C_0)$ vs. reaction time was the rate constant (κ).

3. Results and discussions

3.1. Characterization of HMS/C_3N_4 composites

3.1.1. Morphology

To observe the morphology of the as-synthesized composites and identify material composition of hybrid materials, the morphologies of g-C_3N_4, HMS and HMS/C_3N_4 materials were observed with TEM and shown in Fig. 1. Pure g-C_3N_4 displays a large particles shape with layered structure with numerous stacking layers, and its edge area consists of several sheets, which exhibit a relatively dark brightness (Fig. 1(a)), which was similar to the result reported by Xu et al. [19]. The prepared HMS particles are 50 nm (Fig. 1(b)). When the mixture of HMS and

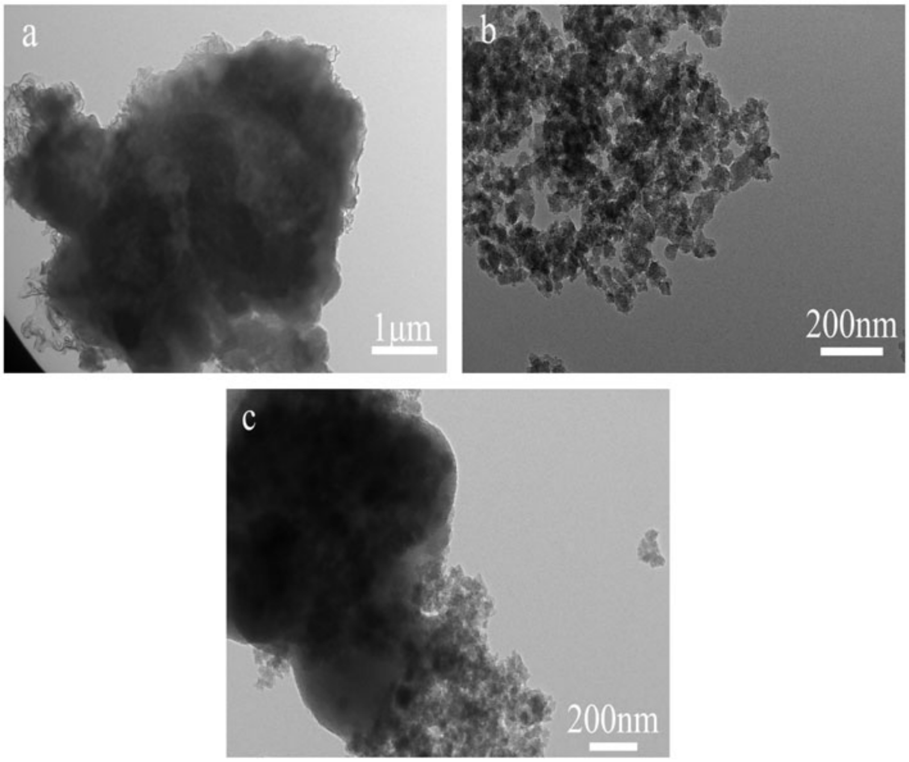

Fig. 1. TEM images of pure-C_3N_4 (a), HMS (b) and HMS/C_3N_4 (c).

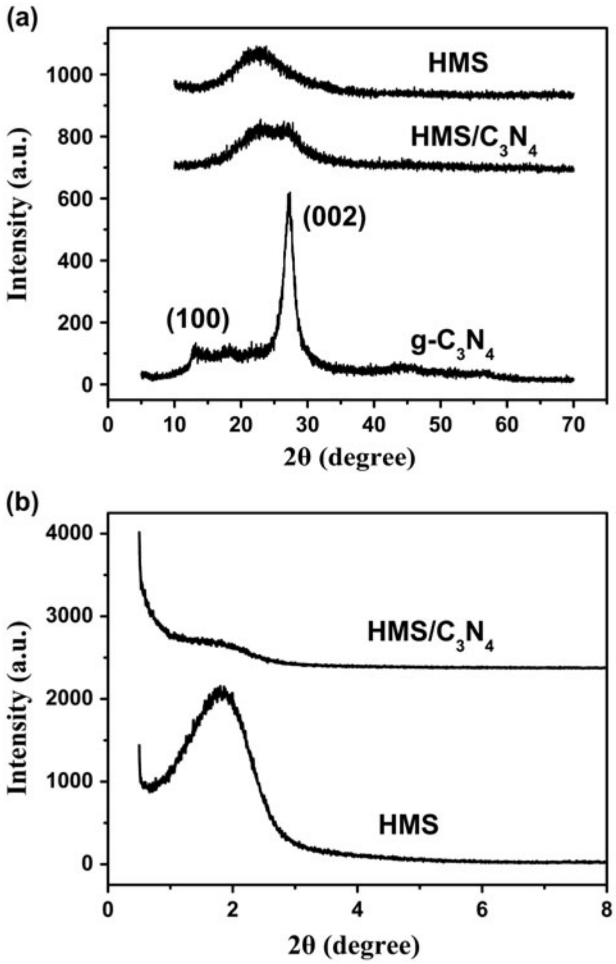

Fig. 2. XRD patterns of HMS, HMS/C_3N_4, and pure-C_3N_4 (a) low-angle XRD patterns of HMS and HMS/C_3N_4 (b).

dicyandiamide was heated to form HMS/C_3N_4, the HMS particles were partly covered by the C_3N_4 from the TEM of HMS/C_3N_4 (Fig. 1(c)).

3.1.2. Crystal phase structure

In order to investigate the crystal phase composition of prepared materials, the XRD patterns of as-made pure C_3N_4, HMS and HMS/C_3N_4 were recorded and shown in Fig. 2(a). HMS had a weak and wide peak at approximately 23° because of its amorphous structure. The XRD pattern of g-C_3N_4 showed a clear peak at 27.4° corresponding to the (0 0 2) interlayer of g-C_3N_4 [20], and there was another small peak at 13° agreed well with the (1 0 0) crystal plane [21]. The XRD pattern of HMS/C_3N_4 showed that there were two peaks at 23° and 27.4°, corresponding to the (0 0 2) interlayer of g-C_3N_4 and HMS. In order to investigate the pore structure, small-angle X-ray diffraction patterns of HMS and HMS/C_3N_4 were presented in Fig. 2(b). From Fig. 2(b), we can see that both HMS and HMS/C_3N_4 samples contain a single low-angle diffraction peak at about $2\theta = 2^\circ$ ascribed to the (1 0 0) crystallographic plane of the hexagonal pore structure [22]. And this result represents a characteristic of the mesoporous structure. However, the intensity of the peak of HMS/C_3N_4 decreases sharply compared to that of HMS, suggesting that the mesoporous structures of HMS/C_3N_4 become less uniform because of the introduction of the C_3N_4 into HMS.

3.1.3. Fourier transform infrared spectra analysis

Fig. 3 displays the FT-IR spectra of HMS, C_3N4, HMS/C_3N_4 and $HMS/7C_3N_4$ materials. It shows that the broad absorption peak of the HMS near 3,440 cm^{-1} is assigned to the stretching vibration of O–H hydroxyl groups. Si–O–Si vibrational mode appears near 870 cm^{-1} and 1,075 cm^{-1}. Absorption bands ranging from 1,240 to 1,639 cm^{-1} are present in C_3N4, HMS/C_3N_4 and $HMS/7C_3N_4$. The peaks at 1,639 and 1,240 cm^{-1} were attributable to C=N and C–N stretching vibration modes, revealing that existence of C_3N_4 in HMS/C_3N_4 materials [23]. The absorption peak at 810 cm^{-1} belongs to the characteristic breathing mode of s-triazine [24]. Based on that, we can deduce that as-synthesized hybrids consist of two components HMS and C_3N_4.

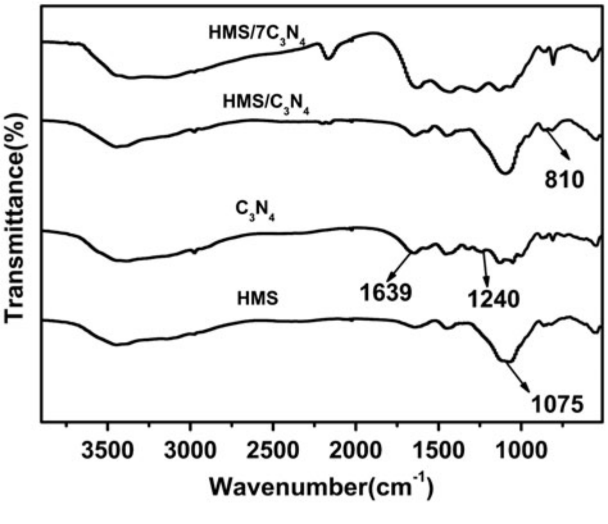

Fig. 3. FT-IR spectra of HMS, C_3N4, HMS/C_3N_4 and $HMS/7C_3N_4$.

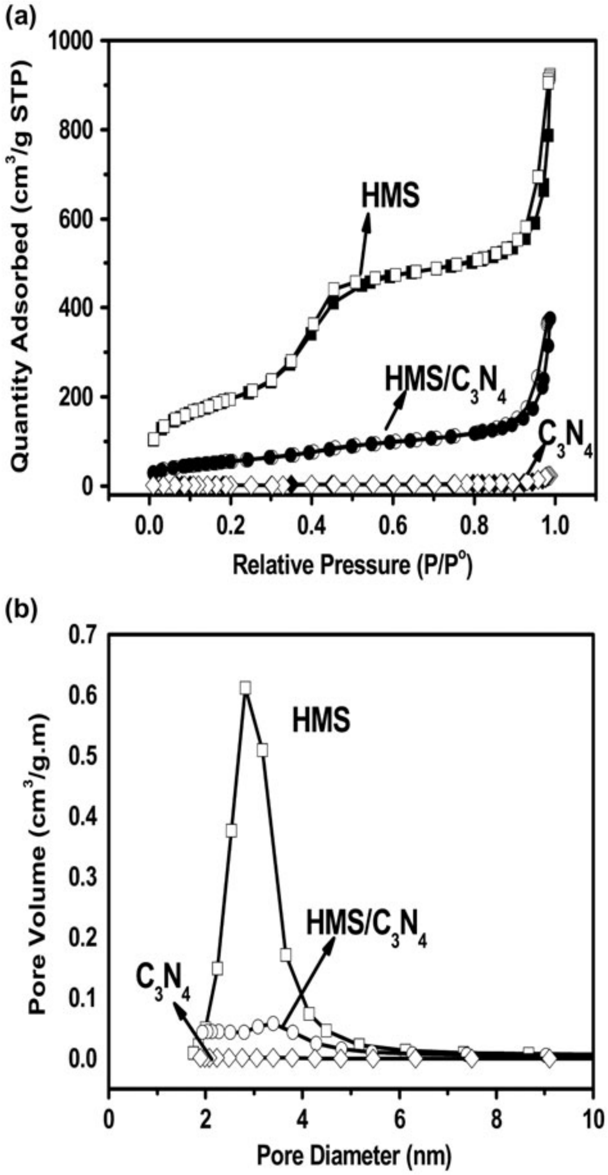

Fig. 4. (a) N_2 adsorption–desorption isotherms and (b) BJH pore size distribution of HMS, HMS/C_3N_4 and pure-C_3N_4. Open and solid symbols represent desorption and adsorption branches, respectively.

3.1.4. BET analysis

To determine the surface area and pore structure of HMS, HMS/C_3N_4 and C_3N_4 and clarify the effect of pore structure on the photocatalytic performance, the N_2 adsorption–desorption isotherm and pore size distribution in the mesopore range corresponding to HMS, HMS/C_3N_4, and C_3N_4 materials are depicted in Fig. 4. The isotherms of HMS, HMS/C_3N_4, and C_3N_4 materials are identified as classical type IV by IUPAC, which is characteristic of mesporous structure (2–50 nm, Fig. 4(a)). The pore distributions of the HMS, HMS/C_3N_4, and C_3N_4 are given in Fig. 4(b). The range of pore sizes is 2.5–3.5 nm, the maximum pore sizes are about 2.84, 2.7, and 2.5 nm, respectively. The Brunauer–Emmett–Teller (BET) surface area and total pore volume of HMS, HMS/C_3N_4, and C_3N_4 were listed in Table 1. The HMS and HMS/C_3N_4 materials had higher BET surface areas of 710.5 and 202.9 m^2/g, respectively, which were much higher than that of C_3N_4 (7.1 m^2/g).

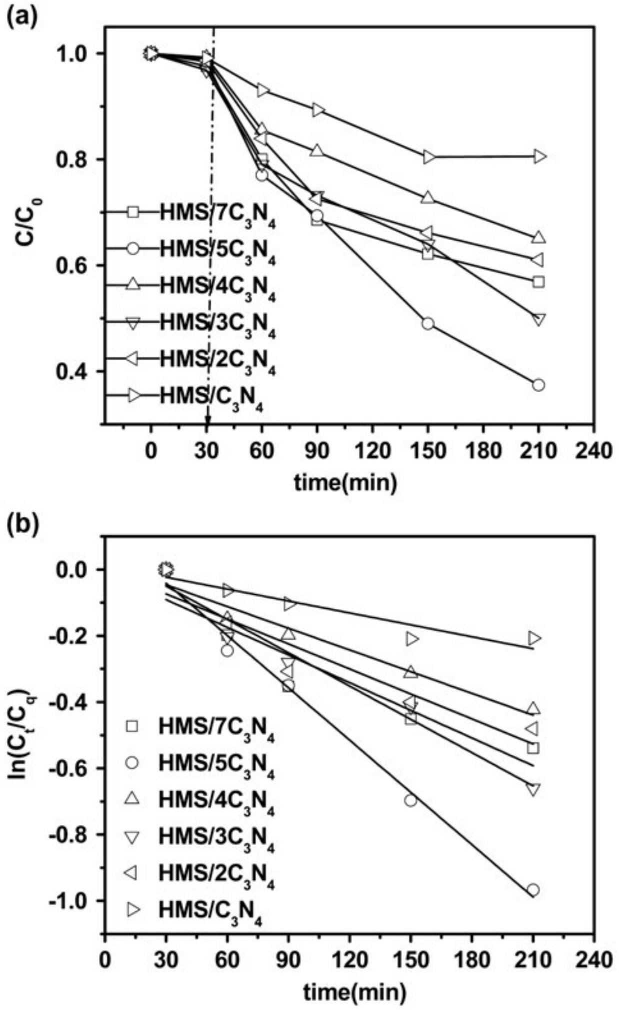

Fig. 5. Photocatalytic decomposition time courses of BPA (initial concentration 5 mg/L) on HMS/7C3N4, HMS/5C3N4, HMS/4C_3N_4, HMS/3C3N4, HMS/2C_3N_4, and HMS/C_3N_4 composites (catalyst dosage 1.0 g/L) (a) and the corresponding first-order plots (b).

3.2. Photocatalytic performance

To investigate the effect of amount of HMS in HMS/C_3N_4 hybrid materials on the photocatalytic degradation of BPA and optimize mass ratio of HMS

Table 1
BET surface area and pore parameters of HMS, HMS/C_3N_4 and pure-C_3N_4

Materials	BET surface area (m^2/g)	Total pore volume (cm^3/g)
HMS	710.5	1.4637
HMS/C_3N_4	202.9	0.5943
Pure g-C_3N_4	7.1	0.0368

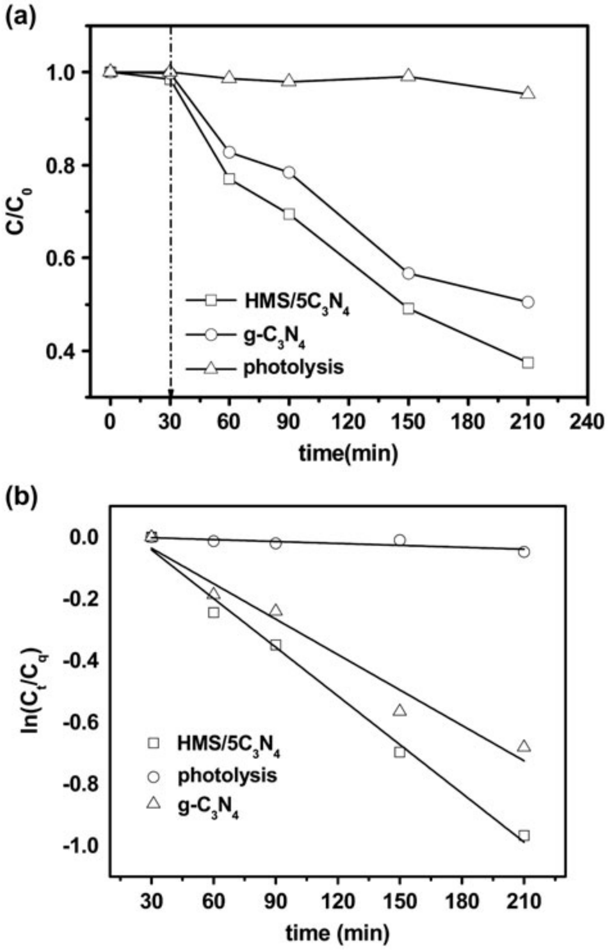

Fig. 6. Direct photolysis (20 W UV light, main wavelength 254 nm) and photocatalytic decomposition time courses of BPA (initial concentration 5 mg/L) on pure-C_3N_4 and HMS/5C_3N_4 composites (a) and the corresponding first-order plots (b).

to dicyandiamide in the preparation process, the photocatalytic degradation of BPA over a series of HMS/C_3N_4 was examined. The experimental condition was 1.0 g/L photocatalyst, 5 mg/L BPA solution and the pH value of BPA solution was 7.0. The photocatalytic decomposition time course of BPA over HMS/C_3N_4, HMS/2C_3N_4, HMS/3C_3N_4, HMS/4C_3N_4, HMS/5C_3N_4, and HMS/7C_3N_4 materials and the corresponding first-order plots were shown in Fig. 5. We can see from Fig. 5(a) that the adsorption removal ratios of BPA on the HMS/C_3N_4, HMS/2C_3N_4, HMS/3C_3N_4, HMS/4C_3N_4, HMS/5C_3N_4, and HMS/7C_3N_4 were lower than 3.0% because C_3N_4 and HMS have no adsorption ability for hydrophobic BPA in water. After light illumination, photocatalytic degradation removal ratios of BPA on HMS/C_3N_4, HMS/2C_3N_4, HMS/3C_3N_4, HMS/4C_3N_4, HMS/5C_3N_4, and HMS/7C_3N_4 were 18.60, 37.60, 46.80, 34.20, 61.0, and 40.70%, respectively. The pseudo-first-order degradation kinetic constants for BPA over the HMS/C_3N_4, HMS/2C_3N_4, HMS/3C_3N_4, HMS/4C_3N_4, HMS/5C_3N_4, and HMS/7C_3N_4 were 0.00120 min, 0.00251, 0.00335, 0.00218, 0.00526, and 0.00278 min^{-1}, respectively (Fig. 5(b)). The rate constant increased from 0.00120 to 0.00526 min^{-1} with the increasing of dicyandiamide to HMS from 1:5 to 5:5. Further increasing the mass ratio of dicyandiamide to HMS from 5:5 to 7:5 in preparation process, the degradation rate constants decreased from 0.00526 to 0.00278 min^{-1}. The main reason maybe that increasing dicyandiamide may produce gradually more C_3N_4, the elevating C_3N_4 with photocatalytic activity can decompose BPA rapidly. However, excess dicyandiamide amount maybe produce excess C_3N_4 in HMS/C_3N_4 materials, which resulted in agglomeration phenomenon of C_3N_4. Hence the optimal mass ratio of dicyandiamide to HMS was 5:5 in the preparation process of the HMS/C_3N_4 materials.

In order to confirm the role of HMS in HMS/C_3N_4, the photocatalytic degradation of BPA over HMS/5C_3N_4, pure C_3N_4 and P25 (commercial standard photocatalyst) and photolysis of BPA were carried out. The degradation conditions were 5 mg/L BPA initial concentration, 1.0 g/L photocatalysts and the solution pH 7.0. Fig. 6 illustrated that photocatalytic decomposition time courses of BPA over these materials and the corresponding first-order plots. Even with the same catalyst dosage (1.0 g/L), the pseudo-first-order degradation kinetic constants of BPA over HMS/5C_3N_4, P25, and pure C_3N_4 were 0.00526, 0.00298, and 0.00383 min^{-1}, respectively. While the rate constant of photolysis was only 0.00021 min^{-1}. The degradation rate constant of BPA over HMS/5C_3N_4 was 1.76 times and 1.4 times than those on P25 and pure C_3N_4, respectively. The experiment results indicated that the HMS in HMS/C_3N_4 hydrid materials can improve the photocatalytic activity of C_3N_4, the main reason maybe that C_3N_4 in HMS/C_3N_4 had higher surface area compared to pure C_3N_4 resulting in higher photocatalytic performace. In addition, as we know, it is difficult to separate and recycle the pure C_3N_4 particles after the pollutant has been removed completely. However, as for the prepared HMS/C_3N_4, the mesoporous silica in the HMS/C_3N_4 has good sedimentation ability, so it can be separated by filtration or centrifugation.

4. Conclusions

In summary, graphitic carbon nitride (g-C_3N_4) as a rising photocatalyst was first immobilized on HMS by simply heating a mixture of self-prepared HMS and dicyandiamide. The crystal phase structure, morphology, surface area, and pore structure of the prepared HMS/g-C_3N_4 was studied. The optimal mass ratio of dicyandiamide to HMS was 5:5 in the preparation process of the HMS/C_3N_4 materials. The prepared HMS/g-C_3N_4 materials were applied to remove the BPA, which is a representative endocrine chemical. The results indicated that the introduction of HMS with high surface area and good sedimentation ability to C_3N_4 can improve the photocatalytic activity and separation ability of C_3N_4. It is an efficient way to deposit the catalyst on the HMS supporter for the removal of pollutants in real water treatment.

Acknowledgments

This work was financially supported by the National Natural Science Foundation of China (No. 21261026), Natural Science Foundation of Yunnan Province (2016FB014), Key Program of Yunnan Province Foundation (2013FA005).

References

[1] X.C. Wang, K. Maeda, X.F. Chen, K. Takanabe, K. Domen, Y.D. Hou, X.Z. Fu, M. Antonietti, Polymer semiconductors for artificial photosynthesis: Hydrogen evolution by mesoporous graphitic carbon nitride with visible light, J. Am. Chem. Soc. 131 (2009) 1680–1681.

[2] T.T. Li, L.L. Zhao, Y.M. He, J. Cai, M.F. Luo, J.J. Lin, Synthesis of g-C_3N_4/$SmVO_4$ composite photocatalyst with improved visible light photocatalytic activities in RhB degradation, Appl. Catal. B: Environ. 129 (2013) 255–263.

[3] Y.M. He, J. Cai, T.T. Li, Y. Wu, Y.M. Yi, M.F. Luo, L.H. Zhao, Synthesis, characterization, and activity evaluation of $DyVO_4$/g-C_3N_4 composites under visible-light irradiation, Ind. Eng. Chem. Res. 51 (2012) 14729–14737.

[4] Y.M. He, Y. Wang, L.H. Zhang, B.T. Teng, M.H. Fan, High-efficiency conversion of CO_2 to fuel over ZnO/g-C_3N_4 photocatalyst, Appl. Catal. B: Environ. 168 (2015) 1–8.

[5] S. Hwang, S. Lee, J.S. Yu, Template-directed synthesis of highly ordered nanoporous graphitic carbon nitride through polymerization of cyanamide, Appl. Surf. Sci. 253 (2007) 5656–5659.

[6] S. Fang, K. Lv, Q. Li, H. Ye, D. Du, M. Li, Effect of acid on the photocatalytic degradation of rhodamine B over g-C_3N_4, Appl. Surf. Sci. (2015), doi: 10.1016/j.apsusc.2015.07.179.

[7] Z. Jin, Q. Zhang, S. Yuan, T. Ohno, Synthesis high specific surface area nanotube g-C_3N_4 with two-step condensation treatment of melamine to enhance photocatalysis properties, RSC Adv. 5 (2015) 4026–4029.

[8] F. Dong, M. Ou, Y.K. Jiang, S. Guo, Z.B. Wu, Efficient and durable visible light photocatalytic performance of porous carbon nitride nanosheets for air purification, Ind. Eng. Chem. Res. 53 (2014) 2318–2330.

[9] Y. Zhang, J. Liu, G. Wu, W. Chen, Porous graphitic carbon nitride synthesized via direct polymerization of urea for efficient sunlight-driven photocatalytic hydrogen production, Nanoscale 4 (2012) 5300–5303.

[10] S. Cao, J. Low, J. Yu, M. Jaroniec, Polymeric photocatalysts based on graphitic carbon nitride, Adv. Mater. (2015), doi: 10.1002/adma.201500033.

[11] Z.H. Tang, X. He, Y. Song, L. Liu, Q.G. Guo, J.H. Yang, Properties of mesoporous carbons prepared from different carbon precursors using nanosize silica as a template, New Carbon Mater. 25 (2010) 465–469.

[12] Y. Li, Y. Sun, F. Dong, W.K. Ho, Enhancing the photocatalytic activity of bulk g-C_3N_4 by introducing mesoporous structure and hybridizing with graphene, J. Colloid Interface Sci. 436 (2014) 29–36.

[13] M. Zhang, J. Xu, R. Zong, Y. Zhu, Enhancement of visible light photocatalytic activities via porous structure of g-C_3N_4, Appl. Catal. B: Environ. 147 (2014) 229–235.

[14] X. Wang, S. Wang, W. Hu, J. Cai, L. Zhang, L. Dong, L. Zhao, Y. He, Synthesis and photocatalytic activity of SiO_2/g-C_3N_4 composite photocatalyst, Mater. Lett. 115 (2014) 53–56.

[15] Y. Chen, K. Wang, L. Lou, Photodegradation of dye pollutants on silica gel supported TiO_2 particles under visible light irradiation, J. Photochem. Photobiol., A 163 (2004) 281–287.

[16] Y. Li, S.J. Kim, Synthesis and characterization of nano titania particles embedded in mesoporous silica with both high photocatalytic activity and adsorption capability, J. Phys. Chem. B 109 (2005) 12309–12315.

[17] Y. Kuwahara, K. Maki, Y. Matsumura, T. Kamegawa, K. Mori, H. Yamashita, Hydrophobic modification of a mesoporous silica surface using a fluorine-containing silylation agent and its application as an advantageous host material for the TiO_2 photocatalyst, J. Phys. Chem. C 113 (2009) 1552–1559.

[18] L.J. Luo, Y. Yang, M. Xiao, L.C. Bian, B. Yuan, Y.J. Liu, F.Z. Jiang, X.J. Pan, A novel biotemplated synthesis of TiO_2/wood charcoal composites for synergistic removal of bisphenol A by adsorption and photocatalytic degradation, Chem. Eng. J. 262 (2015) 1275–1283.

[19] J. Xu, Y. Wang, Y.F. Zhu, Nanoporous graphitic carbon nitride with enhanced photocatalytic performance, Langmuir 29 (2013) 10566–10572.

[20] Q. Gu, Y. Liao, L. Yin, J. Long, X. Wang, C. Xue, Template-free synthesis of porous graphitic carbon nitride microspheres for enhanced photocatalytic hydrogen generation with high stability, Appl. Catal. B: Environ. 165 (2015) 503–510.

[21] Q. Lin, L. Li, S. Liang, M. Liu, J. Bi, L. Wu, Efficient synthesis of monolayer carbon nitride 2D nanosheet with tunable concentration and enhanced visible-light photocatalytic activities, Appl. Catal. B: Environ. 163 (2015) 135–142.

[22] A. Trouvé, I. Batonneau-Gener, S. Valange, M. Bonne, S. Mignard, Tuning the hydrophobicity of mesoporous silica materials for the adsorption of organic pollutant in aqueous solution, J. Hazard. Mater. 201–202 (2012) 107–114.

[23] J.X. Xia, J. Di, S. Yin, H.M. Li, H. Xu, L. Xu, H.M. Shu, M.Q. He, Solvothermal synthesis and enhanced visible-light photocatalytic decontamination of bisphenol A (BPA) by g-C_3N_4/BiOBr heterojunctions, Mater. Sci. Semicond. Process. 24 (2014) 96–103.

[24] S.C. Yan, Z.S. Li, Z.G. Zou, Photodegradation performance of g-C_3N_4 fabricated by directly heating melamine, Langmuir 25 (2009) 10397–10401.